



A One-Dimensional Pt Degradation Model for Polymer Electrolyte Fuel Cells

Yubai Li,^{a,*} Koji Moriyama,^b Wenbin Gu,^c Srikanth Arisetty,^c and C. Y. Wang^{a,**,z}

^aElectrochemical Engine Center (ECEC), and Department of Mechanical and Nuclear Engineering, The Pennsylvania State University, University Park, Pennsylvania 16802, USA

^bHonda R&D Co. Ltd., Haga-machi, Haga-gun, Tochigi, 321-3393 Japan

^cGeneral Motors, Pontiac, Michigan 48340, USA

A one-dimensional model is developed and validated to study platinum degradation and the subsequent electrochemical surface area (ECA) loss in the cathode catalyst layer (CL) of polymer electrolyte fuel cells (PEFCs). The model includes two mechanisms of Pt degradation: Ostwald ripening on carbon support and Pt dissolution-re-precipitation through the ionomer phase. Impact of H₂ | N₂ or H₂ | Air operation, operating temperature, and relative humidity (RH) on Pt degradation during voltage cycling is explored. It is shown that ECA loss is non-uniform across the cathode CL with a zone of exacerbated Pt degradation and hence much lower ECA found near the membrane. This non-uniform Pt degradation is caused by consumption of Pt ions by crossover H₂ in both H₂ | N₂ and H₂ | Air systems. An important consequence is that thinning the cathode electrode in a fuel cell would lead to more ECA loss as a higher fraction of the thin CL would fall in this exacerbated degradation zone. We have quantified the effect of thin cathode CLs on Pt degradation for the first time.

© 2015 The Electrochemical Society. [DOI: 10.1149/2.0101508jes] All rights reserved.

Manuscript submitted March 23, 2015; revised manuscript received April 24, 2015. Published May 7, 2015.

Polymer electrolyte fuel cell (PEFC) durability is a key challenge to commercialization of hydrogen fuel cell vehicles. A central issue of PEFC durability is the loss of electrochemical surface area (ECA) over time. Much research has been carried out in the past two decades¹ to understand the fundamental mechanisms of platinum degradation and to suggest effective mitigation strategies. Four processes have been outlined as possible Pt degradation mechanisms²: i) Ostwald ripening on carbon support;³⁻⁷ ii) Pt crystal migration and coalescence;⁸⁻¹⁰ iii) detachment and agglomeration of Pt nanoparticles induced by carbon corrosion;¹¹⁻¹⁴ and iv) Pt dissolution, Pt ion transport in the ionomer phase and subsequent re-precipitation by H₂ crossover through the membrane.^{4,6,15-18} Although the dominating degradation mechanisms under various fuel cell operating conditions are still under debate, durability test protocols¹⁹ of electrocatalysts, such as those suggested by Fuel Cell Commercialization Conference of Japan (FCCJ), can lend some basic insight into degradation mechanisms. For start/stop durability tests, a triangular-wave potential cycle of 1.0–1.5 V vs. reversible hydrogen electrode (RHE) is chosen and the major degradation is carbon corrosion¹⁹ and the ensuing Pt agglomeration and Pt detachment.²⁰ Suppressing carbon corrosion under such high voltage would be the first priority.^{21,22} On the other hand, a square-wave potential cycle of 0.6–1.0 V vs. RHE is used to simulate the load-cycle tests and Pt degradation induced by carbon corrosion is minor in this case,^{19,23} and Ostwald ripening and Pt dissolution followed by re-precipitation could lead to accelerated degradation.^{4,24} While the present study is limited to modeling Pt degradation under standard test protocols, the model's predictability is expected to extend to actual PEFC operating conditions during vehicle driving.

According to Pourbaix diagram, Pt dissolution can occur at voltages higher than 1.0 V and pH less than 0 at 25°C.²⁵ Mitsushima et al.²⁶ suggested that Pt solubility in acidic media increases with temperature and decreases with pH. It was also observed that the voltage cycling accelerates the dissolution of Pt.²⁷⁻²⁹ Since the PEFCs used in automotive fuel cells involve an acid membrane, and the cathode potential vs. RHE at open circuit voltage is above 1.0 V, the above mentioned degradation mechanisms occur.³⁰ The typical operating temperature of an automotive fuel cell could be as high as 90°C, and the cathode electrode is usually subjected to voltage cycling in a realistic driving cycle.³⁰ Therefore, Pt dissolution is ubiquitous in automotive PEFCs and hence, ECA loss.²⁵

Influences of operating conditions on Pt degradation have been scrutinized in the literature. It was reported that higher

temperature³⁰⁻³⁵ and higher relative humidity (RH)³²⁻³⁷ conditions could induce more rapid Pt degradation. The effect of O₂ partial pressure on the dissolution of Pt nanoparticles has also been investigated.³⁷⁻³⁹ A fundamental study of Matsumoto et al.³⁸ found 18 times accelerated dissolution of polycrystalline Pt under pure O₂ as compared to under pure N₂; however, this acceleration factor decreased to only 1.2 for carbon-supported Pt nanoparticles. Further weakening of the O₂ partial pressure effect was experimentally observed in catalyst layers made of carbon-supported Pt nanoparticles.^{37,39} Indeed, Bi et al.³⁷ reported that the ECA loss under H₂ | N₂ condition is marginally higher than the loss under H₂ | Air condition. This is likely due to the fact that when the O₂ partial pressure increases, the Pt ion sink is pushed farther away from the cathode CL into the membrane, thereby lowering the Pt ion flux dissolved and transported into the membrane.^{40,41} Such a weak effect of O₂ partial pressure on Pt degradation and ECA loss in a fuel cell cathode can only be explained by a one-dimensional model to be developed in the present work.

Another consequence of the combined Pt Ostwald ripening and Pt dissolution-re-precipitation⁴² is non-uniform distribution of degradation across the cathode CL. Indeed, under in-situ voltage cycling test conditions, it was observed that most of Pt mass loss occurred near the CL-membrane interface for both H₂ | N₂^{4,6} and H₂ | Air⁴³ conditions. Moreover, Nagai et al.⁴⁴ carried out durability tests for Pt catalyst on carbon support with different catalyst loadings and hence different CL thickness, and found that a lower Pt loading CL suffers from more rapid ECA loss but the total Pt mass dissolved remains almost the same. Such an observed trend of ECA loss versus CL thickness could be theoretically explained by the possibility that most of the Pt mass loss occurred near the membrane where the Pt ion sink created by crossover H₂ is located, and Pt mass near the GDL is preserved by re-deposition.⁴⁴ However, accurate measurement of ECA loss distribution across the cathode CL is difficult, if possible at all.

Mathematical modeling has been used to aid in deconvoluting Pt degradation mechanisms. Darling and Meyers^{45,46} were the first to develop kinetic rate equations for Pt electrochemical dissolution, Pt oxide film formation, and Pt oxide chemical dissolution. Franco and Tembely⁴⁷ proposed a transient multiscale model of Pt degradation in the cathode electrode using the multi-layer model⁴⁸ of electrochemical interface. Pt degradation under galvanostatic conditions rather than potentiostatic conditions was investigated with this model.⁴⁸ Bi and Fuller⁴⁹ proposed a one dimensional (1D) bi-modal particle size model to investigate the Pt degradation processes, and the mechanism of Pt ion re-precipitation was included. Holby et al.⁵⁰ refined the model of Darling and Meyers⁴⁵ by applying hundreds of particle size groups to represent a nearly continuous PSD. Recently, Ahluwalia et al.³⁵

*Electrochemical Society Student Member.

**Electrochemical Society Active Member.

^zE-mail: cxw31@psu.edu

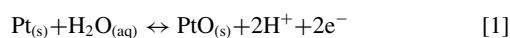
proposed a model hypothesizing that Pt dissolution and subsequent particle agglomeration are responsible for Pt degradation and ECA loss. One significant advance in the work of Ahluwalia et al.³⁵ is that both thermodynamics and kinetics of Pt dissolution are accounted for,⁵¹ as the Pt equilibrium concentration (solubility) could play an important role in Pt dissolution.

Based on the kinetic equations of Holby et al.,^{50,52} a 1D Pt degradation model across the cathode CL is developed in the present work. The present model is focused on the non-uniform Pt degradation distribution and predicts the non-uniform ECA distribution across the cathode CL. The 1D model is used to elucidate the influence of H₂ | N₂ vs. H₂ | Air conditions on Pt degradation in cathode CL and is found to capture well the temperature effects on Pt degradation. Additionally, a new method is introduced to allow the model to capture the humidity effect on both ECA and PSD evolutions. With the capability of predicting both effects of temperature and humidity, the present model is well suited for coupling to a comprehensive fuel cell model⁵³ including electrochemistry, water and heat management and durability in the future. Finally, the Pt degradation as consequence of reducing Pt loading by thinning the CL is quantified.

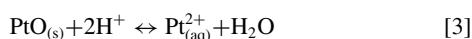
Physical and Numerical Model

The modeling zone is a 1D domain as shown in Fig. 1 where L is the thickness and A is the area of the catalyst layer. The CL-GDL interface is at $x = 0$ and the CL-membrane interface is at $x = L$. Throughout the present study, all Pt particles are assumed to be semi-spherical.

The electrochemical reactions for Pt oxidation and Pt dissolution can be written as:



Additionally, chemical dissolution of Pt oxide may be considered as shown in Eq. 3 (Darling and Meyers⁴⁵):



However, as discussed by Tang et al.⁵⁴ for Pt nanoparticles, the direct electro-oxidation denoted by Eq. 2 is the major dissolution mech-

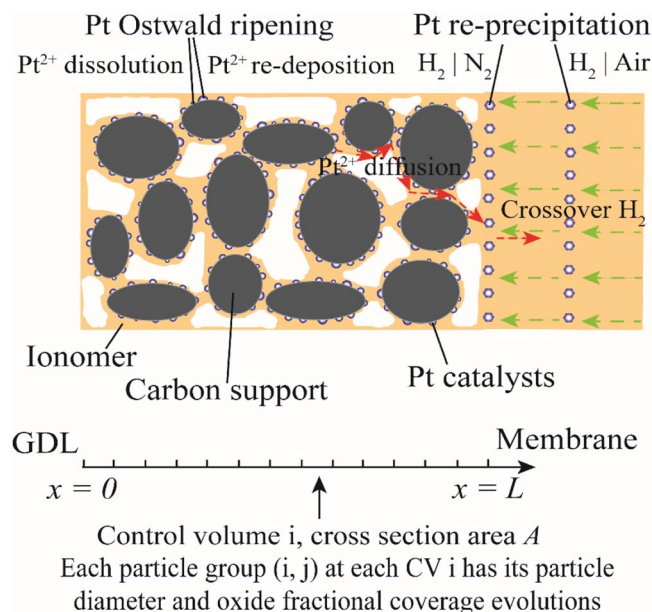


Figure 1. Schematic of 1D Pt degradation model in a PEFC cathode.

anism. Uchimura et al.³⁶ also suggested that the chemical dissolution of Pt oxide is negligible when compared with the electrochemical dissolution of the Pt. Therefore, chemical dissolution of Pt oxides is neglected in this study.

Equations 4–8^{50,52} in the following are used for the current model to capture the PSD and oxide fractional coverage evolutions. The Pt oxide formation and removal is described by a thermo-kinetic rate model developed by Holby and Morgan.⁵² In their model, the forward and backward reaction rates were derived from Eyring-Polanyi equation, and the Brønsted-Evans-Polanyi approach was applied to treat the deviation from equilibrium.⁵² The Pt dissolution and re-deposition was modeled with a modified Butler-Volmer rate equation developed by Holby et al.⁵⁰ Gibbs-Thomson approximation was applied in their model derivation to capture the size dependent stability effect of Pt nanoparticles.⁵⁰ As shown in Fig. 1, the 1D domain can be divided into N control volumes. Assume that on each of the control volume i there are M discrete particle size groups, and one particle size group is denoted by j . The diameter of each particle group is $d_{i,j}$, and the oxide coverage ratio of each particle group is $\theta_{i,j}$. The particle number in each diameter group is $Num_{i,j}$. The particle net oxidation rate $r_{net,oxide}$ [mol/(cm² · s)]⁵² and the net Pt dissolution rate $r_{net,Pt}$ [mol/(cm² · s)]⁵⁰ can be written, respectively, as:

$$r_{net,oxide} = v_1^* \Gamma \exp \left[\frac{-1}{RT} (\bar{H}_{2,fit} + \lambda \theta_{i,j}) \right] \times \left(\left(1 - \frac{\theta_{i,j}}{2} \right) \exp \left[-\frac{n_2 F (1 - \beta_2)}{RT} \left(U_{fit} + \frac{\omega \theta_{i,j}}{n_2 F} - V \right) \right] - \frac{v_2^*}{v_1^*} (10^{-2pH}) \exp \left[\frac{n_2 F \beta_2}{RT} \left(U_{fit} + \frac{\omega \theta_{i,j}}{n_2 F} - V \right) \right] \right) \quad [4]$$

$$r_{net,Pt} = v_1 \Gamma \exp \left[\frac{-\bar{H}_{1,fit}}{RT} \right] (1 - \min(1, \theta_{i,j})) \times \left(\exp \left[-\frac{nF(1 - \beta_1)}{RT} \left(U_{eq} - \frac{4\Omega\gamma_{total}}{d_{i,j}nF} - V \right) \right] - \frac{v_2}{v_1} \frac{c_{Pt^{2+}}}{c_{Pt^{2+}}^{ref}} \exp \left[\frac{nF\beta_1}{RT} \left(U_{eq} - \frac{4\Omega\gamma_{total}}{d_{i,j}nF} - V \right) \right] \right) \quad [5]$$

where the total surface tension γ_{total} [J/cm²] can be expressed as⁵²:

$$\gamma_{total} = \gamma + \Gamma \theta_{i,j} RT \times \left[\log \left(\frac{v_2^*}{v_1^*} \right) + \log (10^{-2pH}) + \frac{n_2 F}{RT} (U_{fit} - V) + \frac{\omega \theta_{i,j}}{2RT} + \log \left(\frac{\theta_{i,j}}{2} \right) + \frac{2 - \theta_{i,j}}{\theta_{i,j}} \log \left(1 - \frac{\theta_{i,j}}{2} \right) \right] \quad [6]$$

The specific descriptions and values of the parameters and physical properties are listed in Table 1. The $c_{Pt^{2+}}$ term in Equation 5 denotes the Pt²⁺ concentration, which can be solved from the 1D Pt²⁺ diffusion equation in this study. For every particle diameter group (i, j) , the particle size and oxide fractional coverage evolutions can be tracked. The initial number of particles in each particle diameter group (i, j) is generated by the initial PSD and the initial total particle number calculated from d_m , the area A and Pt loading. The initial oxide fractional coverage $\theta_{i,j}$ is assumed to be zero in each particle group. The particle diameter evolution rate [cm/s]³⁵ and oxide fractional

Table I. Physical Properties and Parameters.

Symbol	Value	Units	Reference	Description
v_2^*	1×10^4	Hz	Ref. 52	Forward Pt oxide formation rate constant
v_2^*	2×10^{-2}	Hz	Ref. 52	Backward Pt oxide formation rate constant
Γ	2.2×10^{-9}	mol/cm ²	Ref. 52	Pt surface site density
$\bar{H}_{2,fit}$	1.2×10^4	J/mol	Ref. 52	Partial molar oxide formation activation enthalpy(zero coverage)
β_2	0.5		Ref. 52	Butler-Volmer transfer coefficient for Pt oxide formation
n_2	2		Ref. 52	Electrons transferred during Pt oxide formation
U_{fit}	1.03	V	Ref. 52	Pt oxide formation bulk equilibrium voltage
λ	2.0×10^4	J/mol	Ref. 52	Pt oxide dependent kinetic barrier constant
ω	5.0×10^4	J/mol	Ref. 52	Pt oxide-oxide interaction energy
ν_1	1×10^4	Hz	Ref. 52	Dissolution attempt frequency
ν_2	8×10^5	Hz	Ref. 52	Backward dissolution rate factor
β_1	0.5		Ref. 52	Butler-Volmer transfer coefficient for Pt dissolution
n	2		Ref. 52	Electrons transferred during Pt dissolution
U_{eq}	1.118	V	Ref. 52	Pt dissolution bulk equilibrium voltage
Ω	9.09	cm ³ /mol	Ref. 52	Molar volume of Pt
γ	2.4×10^{-4}	J/cm ²	Ref. 52	Pt [1 1 1] surface tension
$c_{Pt^{2+}}^{ref}$	4.0×10^{-3}	mol/L	Fit	Reference Pt ²⁺ concentration
$\bar{H}_{1,fit,100\%RH}$	4.0×10^4	J/mol	Fit	Pt dissolution activation enthalpy under fully humidified condition
K_{H_2}	3.3×10^{-13}	mol/(cm · s · kPa)	Ref. 40	H ₂ permeability at 100% RH and 80°C
K_{O_2}	1.6×10^{-13}	mol/(cm · s · kPa)	Ref. 40	O ₂ permeability at 100% RH and 80°C
p_{H_2}	102.6	kPa	Ref. 40	Partial pressure of H ₂
p_{O_2}	21.5	kPa	Ref. 40	Partial pressure of O ₂
D_{Pt^{2+},H_2O}	10^{-5}	cm ² /s	Ref. 4	Diffusion coefficient of Pt ²⁺ in water
x_{H_2O}	0.4		Ref. 4	Volume fraction of water in ionomer (100% RH)
ε	0.2		Ref. 4	Volume fraction of the ionomer increment in cathode electrode
L	1.0×10^{-3}	cm	Assumed	Thickness of cathode CL if not specified
δ_M	1.8×10^{-3}	cm	Assumed	Thickness of membrane (used for H ₂ Air condition)

coverage development rate [1/s]⁵⁰ can be expressed as:

$$\frac{d(d_{i,j})}{dt} = -r_{net,Pt} \Omega \quad [7]$$

$$\frac{d(\theta_{i,j})}{dt} = \frac{r_{net,oxide}}{\Gamma} - \frac{2\theta_{i,j}}{d_{i,j}} \frac{d(d_{i,j})}{dt} \quad [8]$$

In the current study, because Pt degradation under voltage cycling is of primary interest, the particle diameter growth induced by surface oxides is assumed to be reversible in each potential cycle.⁵⁵ This means that the Pt oxidation and reduction under the voltage cycling does not directly affect the particle diameter evolution, as indicated by Eq. 7. But the oxide fractional coverage can indirectly affect the Pt dissolution rate, as the high oxide fractional coverage at high voltage prohibits Pt from dissolution, as indicated by Eq. 5. Eqs. 7 and 8 are discretized and simulated with classical Runge-Kutta method.

The diffusion equation of Pt²⁺ concentration, $c_{Pt^{2+}}(x)$ [mol/cm³], is given by:

$$\varepsilon \frac{\partial c_{Pt^{2+}}}{\partial t} = \nabla \cdot (\varepsilon^{1.5} D \nabla c_{Pt^{2+}}) + S_{Pt^{2+}} \quad [9]$$

where D is the Pt²⁺ diffusivity in the ionomer. Notice that Pt²⁺ migration occurs with electrolyte potential distribution resulting from current distribution within the electrode. However, its effect can be neglected based on the order of magnitude analysis at a high potential⁴⁹ as well as the simulated low Pt²⁺ concentration at a low potential in this study. As a result, the model is applicable to the actual PEFC undergoing voltage cycling as demonstrated in the Model validation and effects of H₂| air condition section. The diffusivity suggested by Ferreira et al.⁴ is used in this study for the cases under fully humidified condition:

$$D = D_{Pt^{2+},H_2O} x_{H_2O} \quad [10]$$

At the CL-GDL interface, there is no flux boundary condition for $c_{Pt^{2+}}(x)$, i.e.

$$\left. \frac{\partial c_{Pt^{2+}}}{\partial x} \right|_{x=0} = 0 \quad [11]$$

Under the H₂ | N₂ (anode/cathode) condition, a Pt²⁺ sink can be assumed to be exactly at the CL-membrane interface as shown in Fig. 1, as the crossover H₂ will reach this interface without meeting O₂. Thus, the boundary condition at this interface is:

$$c_{Pt^{2+}}|_{x=L} = 0 \quad [12]$$

On the other hand, under the H₂ | Air (anode/cathode) condition, a Pt band forms in the membrane, and the Pt²⁺ concentration can be assumed to be linear from the cathode CL-membrane interface to the Pt band. Then Pt²⁺ concentration boundary condition at the CL-membrane interface is written as:

$$\varepsilon^{1.5} \left. \frac{\partial c_{Pt^{2+}}}{\partial x} \right|_{x=L} = -\frac{c_{Pt^{2+}}}{\delta_{Pt}} \quad [13]$$

where δ_{Pt} is the distance of the Pt band from the cathode CL-membrane interface, which can be estimated as follows⁴⁰:

$$\delta_{Pt} = \frac{2K_{O_2} p_{O_2} \delta_M}{K_{H_2} p_{H_2} + 2K_{O_2} p_{O_2}} \quad [14]$$

where δ_M is the thickness of the membrane, p_{H_2} is the partial pressure of H₂, p_{O_2} is the partial pressure of O₂, while K_{H_2} and K_{O_2} are the permeabilities of H₂ and O₂ through the membrane.

The initial $c_{Pt^{2+}}(x)$ is assumed to be zero throughout the problem domain. Equation 9 is discretized using Implicit Euler and central difference schemes and solved by tridiagonal matrix algorithm (TDMA). In Eq. 9, $S_{Pt^{2+}}(x)$ is the source term due to Pt dissolution. After discretization, this source term of net Pt²⁺ dissolution in each control volume is assumed to be S_i , which can be expressed as:

$$S_i = \sum_{j=1}^M \frac{\pi}{2} \frac{(d_{i,j})^2 \text{Num}_{i,j} r_{net,Pt}}{\Delta v} \quad [15]$$

where Δv is the volume of the control volume:

$$\Delta v = LA/N \quad [16]$$

The geometric surface area (GSA) and the ECA can be calculated by:

$$GSA = 2\pi \sum_{i=1, j=1}^{N, M} Num_{i,j} \left(\frac{d_{i,j}}{2} \right)^2 \quad [17]$$

$$\frac{ECA(t)}{GSA(t)} = \frac{ECA(0)}{GSA(0)} \quad [18]$$

Equation 18 assumes $ECA(t)/GSA(t)$ to be constant⁵² during the degradation process. After the $GSA(t)$ is calculated at each time step, the normalized electrochemical surface area $ECA(t)/ECA(0)$ can be obtained. Similarly, the normalized electrochemical surface area distribution can be calculated as $ECA(x, t)/ECA(x, 0)$.

Results and Discussion

In this section, a comparison of model predictions with the experimental data of Ferreira et al.⁴ is first made. Second, we use the model to explore the effect of O_2 partial pressure. The Pt^{2+} concentration distribution across the cathode CL is found to be affected by the location of the Pt band in the membrane. Consequently, the remaining ECA after voltage cycling is affected by O_2 partial pressure. Third, the temperature effect on ECA evolution is investigated. In addition, an approach to introduce the humidity effect in the current model is developed and validated to capture the ECA and PSD evolutions. Finally, the consequences of lowering the Pt loading through thinning the cathode CL are studied.

Model validation and effects of H_2 | Air condition.— The equilibrium Pt^{2+} concentration is crucial to the understanding of Pt dissolution behavior,² and the modeling of Pt Ostwald ripening behavior⁵⁰ in PEFC. In the Holby et al.⁵⁰ model, the equilibrium concentration data of Bindra et al.⁵⁶ are used. The Pt^{2+} solubility from Bindra et al.'s measurement is with Pt foil⁵⁶ and there exists a strong dependence of Pt equilibrium concentration on the particle size.² Therefore, in the current study, we refitted the value $c_{Pt^{2+}}^{ref}$ with the equilibrium concentration data of Ferreira et al.⁴ Following the approach of Holby and Morgan,⁵² the net dissolution rate should be zero at equilibrium, which means for a nanoparticle of 2.5 nm, the equilibrium concentration at 80°C and 0.95 V is about 1×10^{-6} M.⁴ A major adjusting parameter in this study is the Pt dissolution activation enthalpy $\bar{H}_{1,fit}$. $\bar{H}_{1,fit}$ is adjusted to fit the ECA evolution and PSD distribution from experimental results of Ferreira et al. under 80°C, H_2 | N_2 condition, and the voltage cycles from 0.6 to 1.0 V vs. RHE with sweeping rate of 20 mV/s.⁴ The initial PSD follows a Gauss distribution with mean diameter of $d_m = 3$ nm and variance of $\sigma^2 = 0.22$, and the Pt loading is assumed to be 0.4 mg/cm².⁴ This case is regarded as a baseline in the present paper.

The temporal evolutions of Pt^{2+} concentration near GDL and oxide fractional coverage on a particle of 3 nm near GDL in one (the first) voltage cycle are shown in Fig. 2. In this cycle, the Pt^{2+} concentration reaches about 1.24 μ M when the voltage reaches 1.0 V, which is a reasonable value considering the Pt^{2+} solubility limit at 80°C and 1.0 V (about 0.8–1.5 μ M).⁴ Another finding from this calculation is that the Pt^{2+} concentration is only large under high voltage and is negligible when the voltage is lower than 0.85 V in this voltage cycle. On the other hand, the current density is small at voltage higher than 0.85 V.⁴⁹ So the Pt^{2+} electro-osmotic migration effect driven by potential drop is neglected in the current study, as shown in Eq. 9. Then, $\bar{H}_{1,fit}$ is adjusted and a test of 10,000 voltage cycles is performed. As this calculation is under fully humidified condition, this value of $\bar{H}_{1,fit}$ is defined as $\bar{H}_{1,fit,100\%RH}$ and is used in the following sections. The predicted ECA evolution is in good agreement with the experimental result⁴ as shown in Fig. 3. The remaining Pt mass distribution on carbon support after cycling is compared in Fig. 4. Both experimental and predicted results show non-uniform Pt mass loss, and the highest Pt mass losses are near the CL-membrane interface. A Pt mass depletion region could be found near the CL-membrane

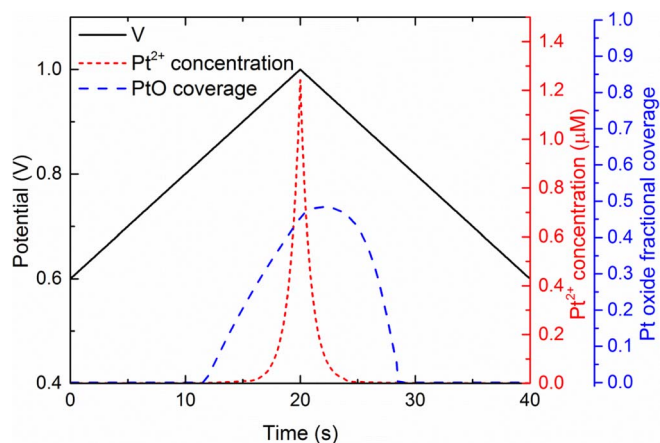


Figure 2. Voltage, Pt^{2+} concentration and PtO fractional coverage evolutions in one voltage cycle.

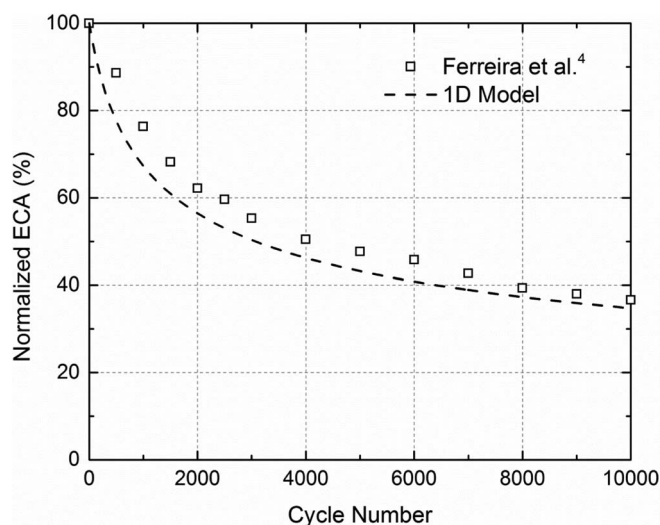


Figure 3. Comparison of predicted and experimental (46 wt% Pt/Vulcan, 0.4 mg/cm² cathode)⁴ ECA evolutions under 0.6 V–1.0 V vs. RHE, 20 mV/s, 80°C, fully humidified H_2 | N_2 (anode/cathode) condition.

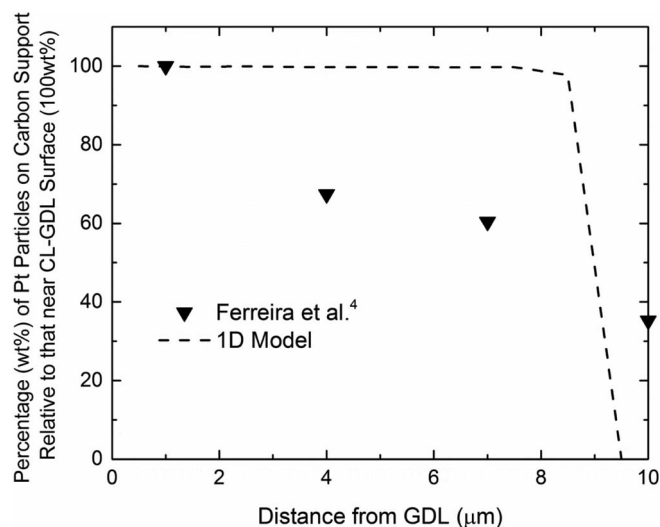


Figure 4. Comparison of predicted and measured (46 wt% Pt/Vulcan, 0.4 mg/cm² cathode)⁴ Pt mass remaining on carbon support under 0.6 V–1.0 V vs. RHE, 20 mV/s, 80°C, fully humidified H_2 | N_2 (anode/cathode) condition.

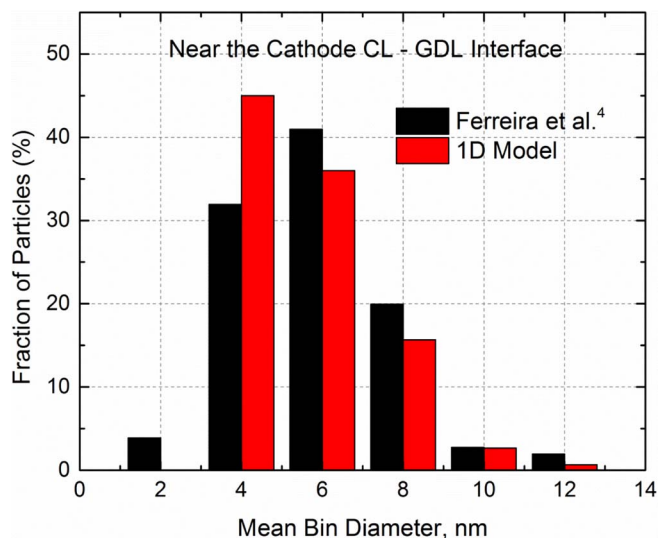


Figure 5. Comparison of predicted and measured (46 wt% Pt/Vulcan, 0.4 mg/cm² cathode)⁴ Pt PSDs remaining on carbon support near CL-GDL interface under 0.6 V–1.0 V vs. RHE, 20 mV/s, 80°C, fully humidified H₂ | N₂ (anode/cathode) condition.

interface, as the soluble Pt²⁺ ion meets H₂, then re-precipitates and nucleates on the large Pt particles in the ionomer phase near this interface.⁴ In our model, the Pt mass depletion region is narrower than that seen in the experiments of Ferreira et al.⁴ where a lot of large Pt particles off carbon support could be found deep within the cathode CL. On the contrary, the current study assumed Pt re-precipitation to occur only at the CL-membrane interface. These large Pt particles off carbon support could induce Pt re-precipitation in the cathode CL, which is neglected in the current study. There could be one possible implication. If the cathode CL is so thin as to be totally under the Pt mass loss region, much faster Pt degradation and overall ECA loss could be found. This is a possible limitation for very thin cathode CLs and will be discussed in detail later. For the PSD, the comparison is only made near the CL-GDL interface, as Pt particles off carbon support can be found at other places across the cathode CL⁴ and our model could only account for Pt particles on carbon support. This comparison of PSD is shown in Fig. 5.

The Pt²⁺ sink created by crossover H₂ will lead to non-uniform Pt²⁺ concentration across the cathode CL and non-uniform ECA loss. The Pt²⁺ concentration distribution in one voltage cycle is shown in Fig. 6a. As crossover H₂ could reach the cathode CL-membrane interface under H₂ | N₂ condition, the Pt²⁺ sink described by Eq. 12 causes a region of lower Pt²⁺ region near membrane. Under H₂ | Air condition described by Eq. 13, the Pt²⁺ sink is in the membrane and the corresponding Pt²⁺ concentration distributions in one voltage cycle are shown in Fig. 6b. Consequently, another case study to investigate the effect of H₂ | Air condition is performed and compared with the baseline. The overall ECA loss is compared in Fig. 7, and it can be found that the overall remaining ECA under H₂ | Air condition is slightly higher than under H₂ | N₂ condition. This finding is in accordance with experimental results of Bi et al.³⁷ Further, our model revealed that Pt mass lost into the ionomer/membrane occurs through dissolution into Pt²⁺, diffusion and subsequent re-precipitation inside the membrane under the H₂ | Air condition, whereas the dissolved Pt²⁺ ions re-precipitate immediately at the CL-membrane interface in the H₂ | N₂ case. Consequently, Pt mass loss into the ionomer/membrane is stronger under H₂ | N₂ condition than that under the H₂ | Air, with the former calculated at 10.2% after 10,000 cycles versus 0.8% for the latter.

The effect of O₂ partial pressure on Pt degradation and ECA loss is clearly explained through the present modeling study. The different boundary conditions at the CL-membrane interface under H₂ | N₂ and

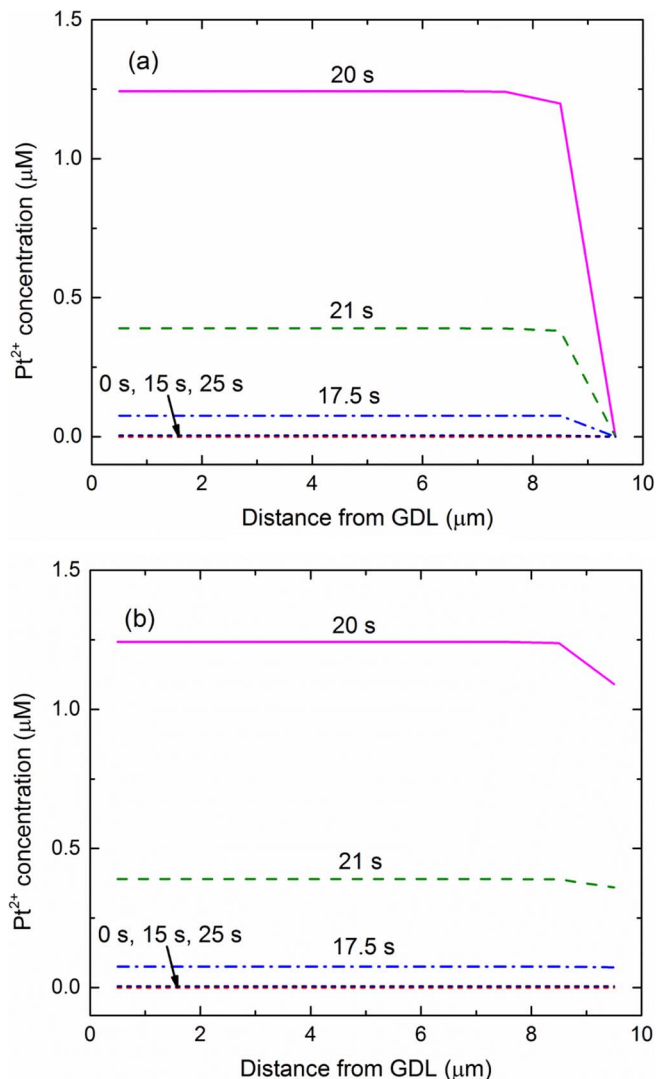


Figure 6. Pt²⁺ concentration distributions in one voltage cycle under: (a) H₂ | N₂ (anode/cathode) and (b) H₂ | Air (anode/cathode) condition.

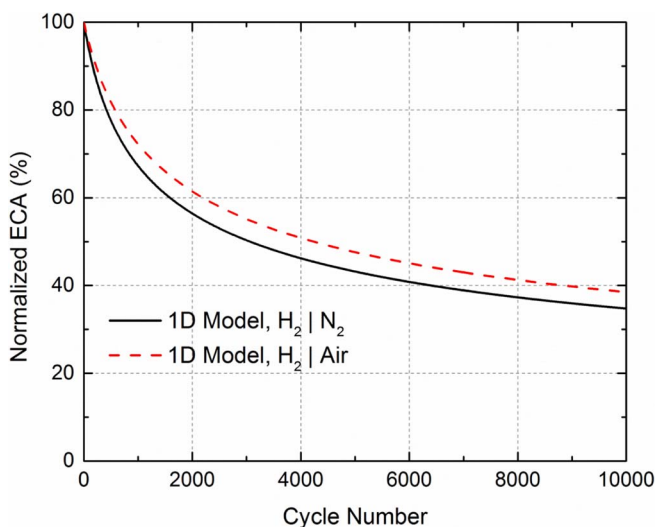


Figure 7. Comparison of ECA evolutions under 0.6 V–1.0 V vs. RHE, 20 mV/s, 80°C, fully humidified H₂ | N₂ (anode/cathode) and H₂ | Air (anode/cathode) condition.

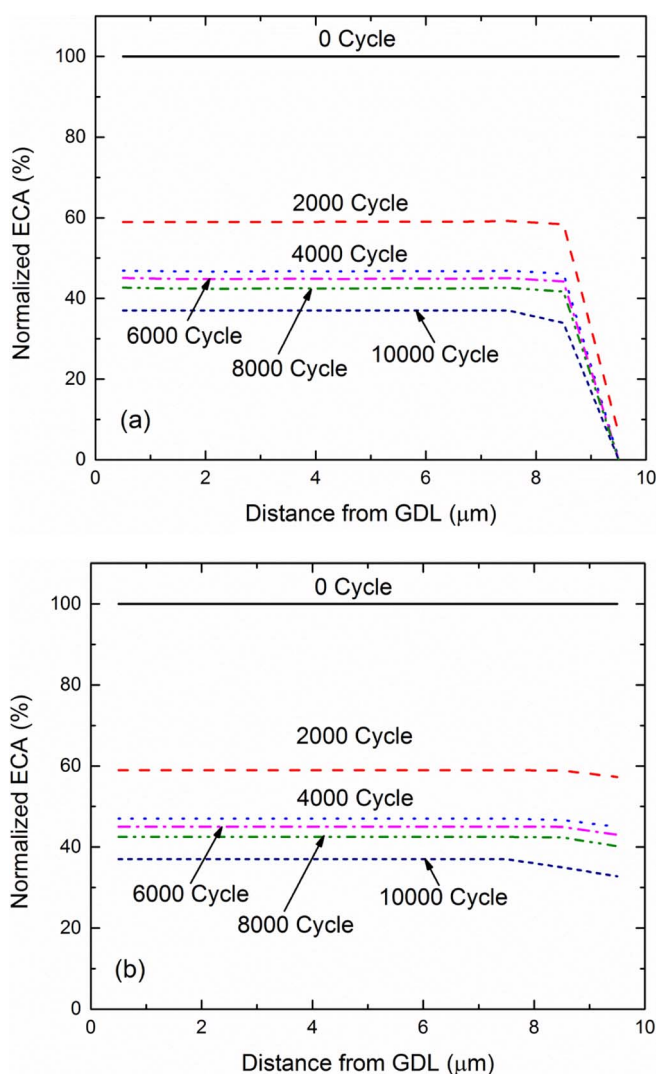


Figure 8. ECA distributions through voltage cycling test under 0.6 V–1.0 V vs. RHE, 20 mV/s, 80°C, fully humidified (a) H₂ | N₂ (anode/cathode) and (b) H₂ | Air (anode/cathode) condition.

H₂ | Air conditions, respectively, lead to differing Pt²⁺ concentration distributions shown in Fig. 6, leading to different remaining ECA distributions shown in Fig. 8. For both cases, faster ECA loss can be found near the cathode CL-membrane interface. The ECA distribution across the cathode CL is difficult to measure experimentally, so the current model offers an alternative to investigate the through-plane non-uniform distribution of ECA loss in the cathode CL.

Temperature and humidity effects.— Several series of experimental data are used to demonstrate the predictability of this model under different temperatures and relative humidity (RH). First, a series of experimental results are used to test whether this model could capture temperature effects on Pt degradation quantitatively. In these tests, square wave potentials are applied on all cycling experiments (25 cm² subscale cells, catalyst loading of 0.35 mg/cm²) under fully humidified H₂ | N₂ condition with voltage hold time of 10 s at 0.95 V and 2.5 s at 0.6 V vs. RHE.³⁰ The only variable in these experiments is the cell temperature, i.e. 40°C, 60°C, and 80°C. The cathode CL thickness and initial PSD are assumed to be identical to those used in the last section. As shown in Fig. 9, the ECA evolutions predicted by the model are in good accordance with the experimental results, indicating that temperature effects are quantitatively captured by this

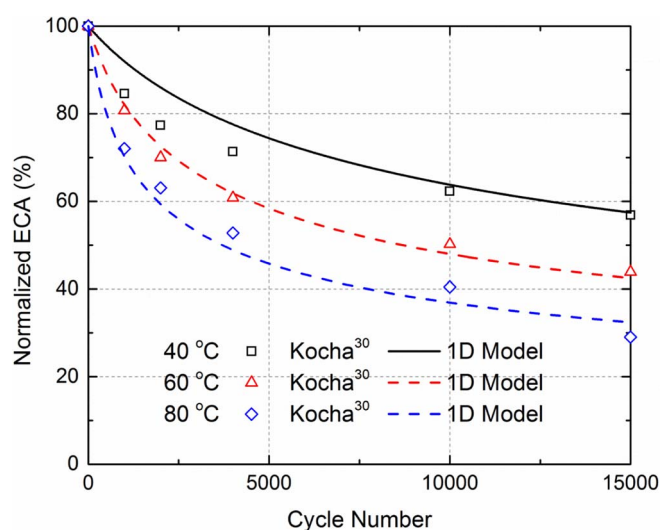


Figure 9. Comparison of predicted and measured (46 wt%, Pt/C, 0.35 mg/cm² cathode)³⁰ ECA evolutions under 10 s hold at 0.95 V, 2.5 s hold at 0.6 V vs. RHE, fully humidified H₂ | N₂ (anode/cathode) condition at various temperatures.

model. The temperature impact on the diffusion coefficient of Pt²⁺ has been neglected in the current stage of study.

Up to this point, all the work deals with Pt degradation under fully humidified condition. This part of study further concerns Pt degradation at low humidity condition. As the proton diffusivity in the ionomer phase is a strong function of RH, the current study assumes that the Pt²⁺ diffusivity follows the same function of proton conductivity with RH.⁵⁷

$$D = D_{\text{Pt}^{2+}, \text{H}_2\text{O}^x \text{H}_2\text{O}} RH^{2.84} \quad [19]$$

Then, as suggested by Ahluwalia et al.,³⁵ the Pt dissolution rate can be written as a function of RH. One hypothesis is that the lower RH restricts the solvation of Pt²⁺ by H₂O and therefore suppresses Pt dissolution.³⁴ Assume a linear correlation as follows:

$$\bar{H}_{1, fit} = \bar{H}_{1, fit, 100\% RH} [C(1 - RH) + 1] \quad [20]$$

where the coefficient C is fitted from experimental data. Uchimura et al.³⁶ performed a series of experimental tests (25 cm² subscale cells, catalyst loading of 0.35 mg/cm²) to investigate the RH effects on the ECA evolutions. The temperature is held constant at 80°C, the upper potential is held for 10 s at 0.95 V vs. RHE and the lower potential is held for 2.5 s at 0.6 V vs. RHE. In addition to the test under 100% RH, two other tests are conducted under 30% and 70% RH. Thus, $\bar{H}_{1, fit, 30\% RH}$ and $\bar{H}_{1, fit, 70\% RH}$ can be found by fitting the 30% and 70% RH results as shown in Fig. 10. Using the least square fitting method, we find $C = 0.3$. The following correlation is thus developed to account for the humidity effect on Pt degradation:

$$\bar{H}_{1, fit} = \bar{H}_{1, fit, 100\% RH} [0.3(1 - RH) + 1] \quad 0.3 \leq RH \leq 1.0 \quad [21]$$

Finally, to demonstrate the effectiveness of the above correlation and the current model, a series of parametric studies are performed and compared with the experimental results from Yang et al.³⁴ who did a series of tests to investigate parametric impacts on cathode CL degradation. The electrode thickness is estimated to be about 10 μm from their post-test microscopy images. Their base case uses square wave potential cycle which holds 10 s at 0.95 V and holds 10 s at 0.4 V vs. RHE. The cell temperature is 80°C and the RH is 100%. Three other experiments are conducted in their study. The low-humidity test only lowers the RH to 30%, the high temperature test only raises the operating temperature to 90°C and the higher upper potential test only raises the higher upper potential to 1.05 V compared with the base study. The Pt loading of the cathode is 0.2 mg/cm², and the

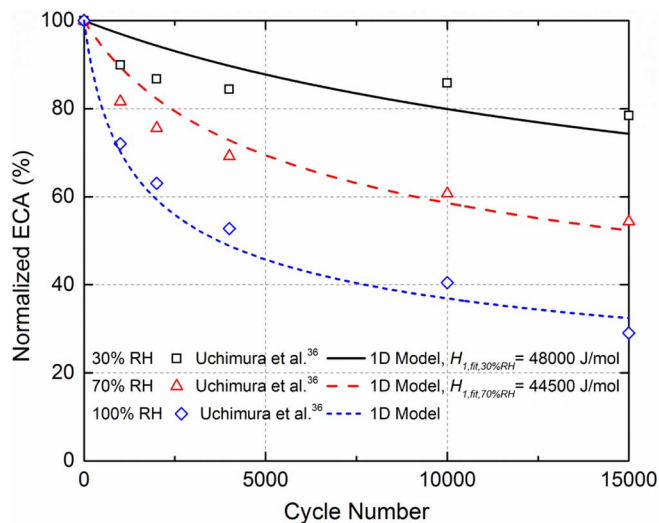


Figure 10. Comparison of predicted and measured (46 wt%, Pt/C, 0.35 mg/cm² cathode)³⁶ ECA evolutions under 10 s hold at 0.95 V, 2.5 s hold at 0.6 V vs. RHE, 80°C, H₂ | N₂ (anode/cathode) condition at various RH.

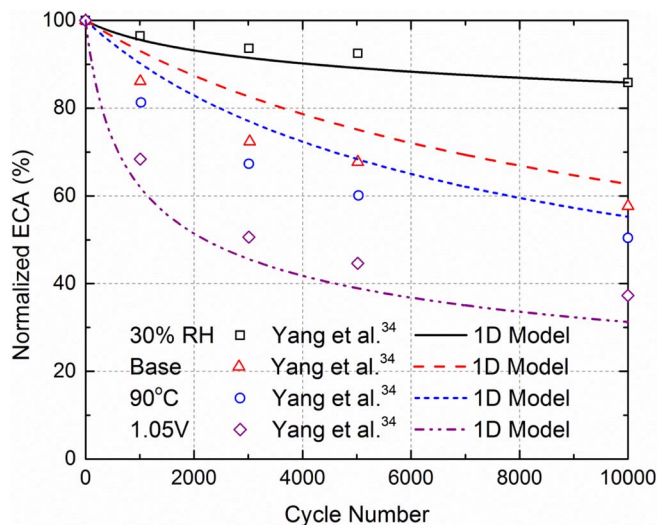


Figure 11. Comparison of predicted and measured (40 wt%, Pt/C, 0.2 mg/cm² cathode)³⁴ ECA evolutions.

PSD of the pristine sample for these cases is measured with TEM and reported.³⁵ As a result, the PSD from TEM measurement³⁵ is applied as the initial PSD in the present model. The correlation expressed by Eq. 21 is used to determine $\bar{H}_{1,fit}$. The overall ECA evolutions are compared with experimental results³⁴ in Fig. 11. And the remaining PSDs at the middle of the cathode electrode are compared with TEM

measurement⁵⁸ as shown in Fig. 12. The current model is found to reasonably capture the impact of RH on both ECA and PSD evolutions. It is worthwhile to note that only a rough estimation of Pt²⁺ diffusivity with RH is used in the current study. It would be helpful to establish a correlation of Pt²⁺ diffusivity with both temperature and RH for further understanding of the Pt degradation in cathode CL.

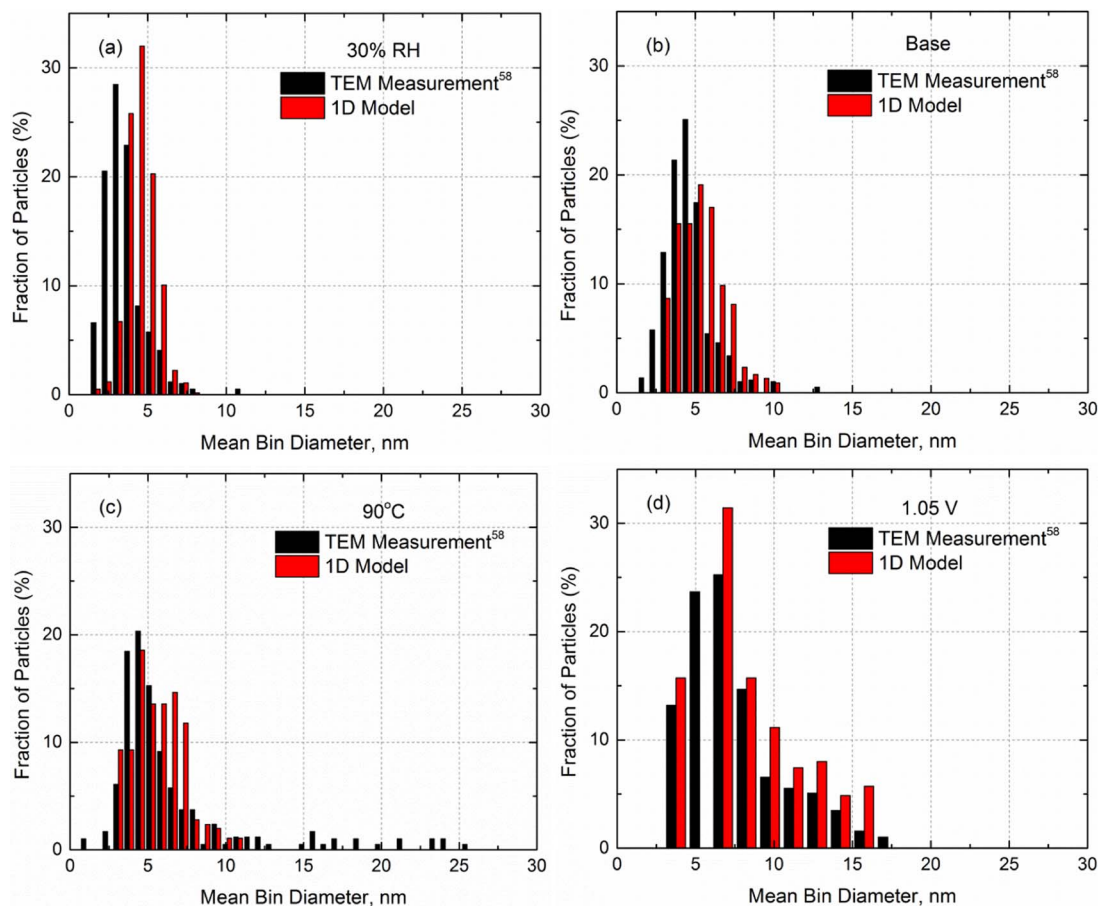


Figure 12. Comparison of analytical carbon-supported PSDs (near CL-GDL interface) with TEM measurements (40 wt%, Pt/C, 0.2 mg/cm² cathode)⁵⁸ after 10,000 voltage cycles.

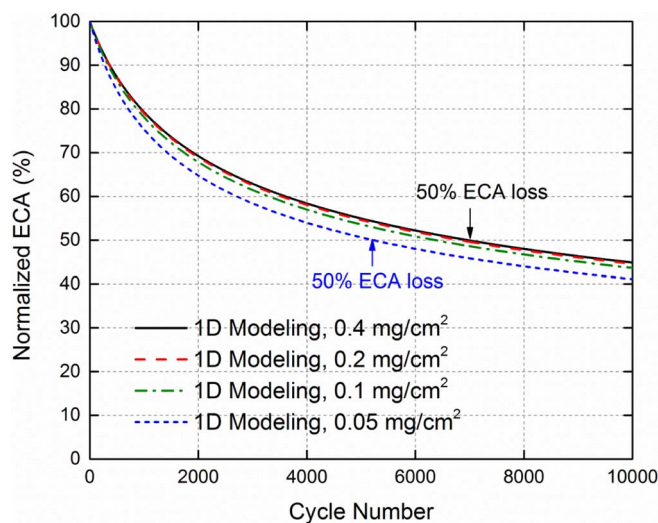


Figure 13. Comparison of ECA evolutions with thinner cathode CLs under 0.6 V–1.0 V vs. RHE, 20 mV/s, 60°C, fully humidified H₂ | N₂ (anode/cathode) condition.

In realistic PEFCs, the temperature field⁵⁹ and RH field⁶⁰ are highly non-uniform in cathode CL, hence spatially non-uniform Pt degradation commonly results. The current study paves the way to couple the Pt degradation model with a comprehensive fuel cell model, which has made significant contributions to elucidate the underlying mechanisms and to greatly increase the performance of PEFC in the last few decades.⁶¹ Although in Fig. 11 and Fig. 12 the Pt degradation trends under various parametric conditions are captured well, more research is warranted. For example, the effects of the voltage cycling frequency,³³ voltage gap,³⁶ or voltage shape³⁹ have not been looked at in the present work. All these actually have profound impacts on Pt dissolution and Pt degradation. Further effort to understand the fundamental mechanisms of Pt dissolution is needed.

Thinning cathode CL effect.— In the last decade, significant advances have been made in reducing Pt loading in PEFC.¹ Gasteiger et al.⁶² demonstrated that in state-of-the-art MEAs operated with H₂ and air, the anode Pt loading can be reduced to 0.05 mg/cm² and the cathode loading can be reduced to 0.20 mg/cm² with a voltage loss of only 20 mV. Researchers then applied advanced Pt dispersion techniques to develop CLs with thickness of several microns⁶³ to less than 1 micron⁶⁴ to reduce Pt loading. Reducing Pt loading is vital to the PEFC cost reduction,⁶⁵ however, it is found that there is large performance decay for low Pt loading CLs caused by the O₂ transport resistance at the ionomer thin film near the Pt surface.^{66–69} Besides the increase of O₂ transport loss, more rapid Pt degradation and ECA loss has also been found for thin CLs in a recent experimental study.⁷⁰ The present study attempts to explain and quantify how the cathode CL thinning would affect the degradation.

A case under 0.6 V–1.0 V vs. RHE, 20 mV/s, 60°C, fully humidified H₂ | N₂ condition is chosen as the starting point for this part of the study, as it is found to experience moderate Pt degradation during the 10,000 cycle period. For this case, the cathode electrode has Pt loading of 0.4 mg/cm², and thickness of 10 μm. Then a series of thinner CLs are modeled. These thinner CLs have thicknesses of 5 μm, 2.5 μm, and 1.25 μm, consequently, the corresponding Pt loadings are 0.2 mg/cm², 0.1 mg/cm², and 0.05 mg/cm². The ECA evolutions are compared in Figure 13 and a clear trend that thinning the cathode CL leads more rapid ECA loss can be seen. The acceleration of degradation is not significant when thinning the CL from 10 μm to 5 μm, however, it becomes important when thinning the CL further to 2.5 μm and 1.25 μm. If 50% of the overall ECA loss is chosen as a failure criterion, the electrode with 0.4 mg/cm² Pt loading could

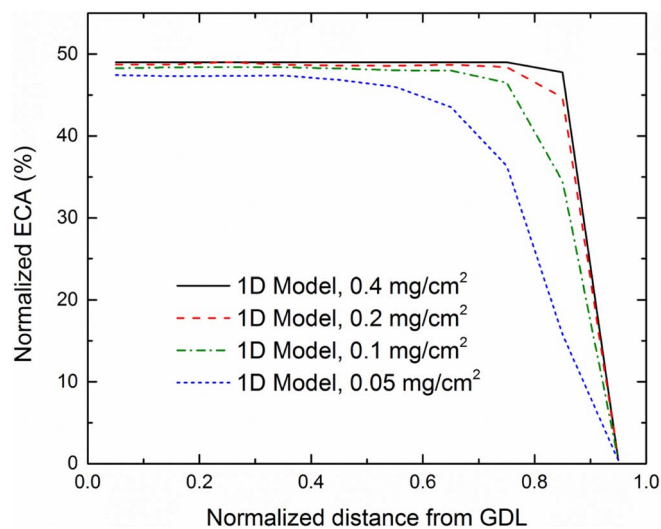


Figure 14. Comparison of ECA distributions after cycling with thinner cathode CLs under 0.6 V–1.0 V vs. RHE, 20 mV/s, 60°C, fully humidified H₂ | N₂ (anode/cathode) condition.

last 7,000 cycles, however, the electrode with 0.05 mg/cm² Pt loading could only last 5,200 cycles – a 26% reduction in durability.

In the previous modeling cases, an exacerbated degradation region is found near the membrane, which is caused by the lower Pt²⁺ concentration in this region due to Pt²⁺ sink, as seen in Fig. 14 which shows the ECA distributions under normalized CL thicknesses. For the thinned CL, a larger fraction of the CL thickness is under the exacerbated degradation region and faster ECA loss can be found throughout the CL. The present study clearly suggests that the faster Pt degradation is a limitation for lowering the cathode Pt loading by thinning the cathode CL.

The uneven variation in ECA across the catalyst layer can be comprehended by comparing PSDs across the cathode CL. Fig. 15 shows the PSDs at four different locations for the electrode with 0.05 mg/cm² Pt loading and 1.25 μm thickness. Although the initial PSD at each position is identical, the variation in PSD along the cathode CL thickness could be clearly seen in Fig. 15 after 10,000 voltage cycles. The model calculates that larger Pt particles will be near CL-GDL interface due to less impact from Pt²⁺ diffusion into the membrane.

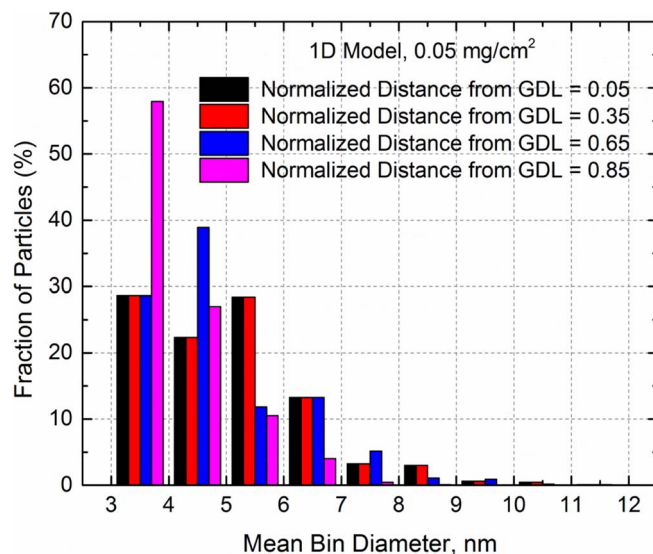


Figure 15. Analytical carbon-supported PSDs across a cathode CL after 10,000 cycles under 0.6 V–1.0 V vs. RHE, 20 mV/s, 60°C, fully humidified H₂ | N₂ (anode/cathode) condition.

Therefore particles grow more at the CL-GDL interface primarily due to re-deposition from available Pt²⁺. To sum up, the current model offers a quantitative approach to investigate non-uniform Pt degradation across the cathode CL.

Conclusions

In the current study, a 1D Pt degradation model is developed and validated. Slightly faster degradation is found for the cathode CL under H₂ | N₂ than under H₂ | Air condition, as the Pt²⁺ sink moves into the membrane under H₂ | Air condition instead of at the cathode CL-membrane interface under H₂ | N₂ condition. The temperature effect on ECA evolution is well captured by the current model. In addition, a new approach to capture RH effect on Pt degradation is developed and compared with experimental results. Thus, the current model of Pt degradation is extended to work under low-humidity conditions. Due to the non-uniform Pt²⁺ concentration distribution across a CL, the ECA loss is found to be non-uniform across the CL as predicted by the current model. Exacerbated degradation could be found near the CL-membrane interface. One important consequence is that thinning the cathode CL would induce more rapid ECA loss. This new physical insight is quantitatively explored with the current model. When the cathode thickness is reduced from 10 μm to 5 μm, the accelerated degradation is insignificant. However, when the cathode thickness is further reduced to 2.5 μm and 1.25 μm, the apparent accelerated ECA loss is predicted, suggesting that worsen Pt degradation could be a limitation in thinning the cathode catalyst layer to achieve low or ultra-low Pt loading.

References

- R. Borup, J. Meyers, B. Pivovar, Y. S. Kim, R. Mukundan, N. Garland, D. Myers, M. Wilson, F. Garzon, and D. Wood, *Chem. Rev. (Washington, DC)*, **107**, 3904 (2007).
- Y. Shao-Horn, W. C. Sheng, S. Chen, P. J. Ferreira, E. F. Holby, and D. Morgan, *Top. Catal.*, **46**, 285 (2007).
- J. Aragane, H. Urushibata, and T. Murahashi, *J. Appl. Electrochem.*, **26**, 147 (1996).
- P. J. Ferreira, G. J. la O', Y. Shao-Horn, D. Morgan, R. Makharia, S. Kocha, and H. A. Gasteiger, *J. Electrochem. Soc.*, **152**, A2256 (2005).
- A. V. Virkar and Y. Zhou, *J. Electrochem. Soc.*, **154**, B540 (2007).
- S. Chen, H. A. Gasteiger, K. Hayakawa, T. Tada, and Y. Shao-Horn, *J. Electrochem. Soc.*, **157**, A82 (2010).
- C. E. Carlton, S. Chen, P. J. Ferreira, L. F. Allard, and Y. Shao-Horn, *J. Phys. Chem. Lett.*, **3**, 161 (2012).
- M. S. Wilson, F. H. Garzon, K. E. Sickafus, and S. Gottesfeld, *J. Electrochem. Soc.*, **140**, 2872 (1993).
- H. L. Xin, J. A. Mundy, Z. Liu, R. Cabezas, R. Hovden, L. F. Kourkoutis, J. Zhang, N. P. Subramanian, R. Makharia, F. T. Wagner, and D. A. Muller, *Nano Lett.*, **12**, 490 (2012).
- Y. Yu, H. L. Xin, R. Hovden, L. Wang, E. D. Rus, J. A. Mundy, D. A. Muller, and H. D. Abruna, *Nano Lett.*, **12**, 4417 (2012).
- R. Makharia, S. S. Kocha, P. T. Yu, M. A. Sweikart, W. Gu, F. T. Wagner, and H. A. Gasteiger, *ECS Trans.*, **1** (8), 3 (2006).
- K. J. J. Mayrhofer, J. C. Meier, S. J. Ashton, G. K. H. Wiberg, F. Kraus, M. Hanzlik, and M. Arenz, *Electrochem. Commun.*, **10**, 1144 (2008).
- K. J. J. Mayrhofer, S. J. Ashton, J. C. Meier, G. K. H. Wiberg, M. Hanzlik, and M. Arenz, *J. Power Sources*, **185**, 734 (2008).
- A. A. Franco and M. Gerard, *J. Electrochem. Soc.*, **155**, B367 (2008).
- P. Yu, M. Pemberton, and P. Plasse, *J. Power Sources*, **144**, 11 (2005).
- K. Yasuda, A. Taniguchi, T. Akita, T. Ioroi, and Z. Siroma, *J. Electrochem. Soc.*, **153**, A1599 (2006).
- T. Akita, A. Taniguchi, J. Maekawa, Z. Siroma, K. Tanaka, M. Kohyama, and K. Yasuda, *J. Power Sources*, **159**, 461 (2006).
- K. Yasuda, A. Taniguchi, T. Akita, T. Ioroi, and Z. Siroma, *Phys. Chem. Chem. Phys.*, **8**, 746 (2006).
- A. Ohma, K. Shinohara, A. Iiyama, T. Yoshida, and A. Daimaru, *ECS Trans.*, **41**(1), 775 (2011).
- J. C. Meier, C. Galeano, I. Katsounaros, A. A. Topalov, A. Kostka, F. Schüth, and K. J. J. Mayrhofer, *ACS Catal.*, **2**, 832 (2012).
- P. T. Yu, W. Gu, R. Makharia, F. T. Wagner, and H. A. Gasteiger, *ECS Trans.*, **3**(1), 797 (2006).
- A. Taniguchi, T. Akita, K. Yasuda, and Y. Miyazaki, *J. Power Sources*, **130**, 42 (2004).
- A. Zana, J. Speder, M. Roefzaad, L. Altmann, M. Bäumer, and M. Arenz, *J. Electrochem. Soc.*, **160**, F608 (2013).
- F. T. Wagner, S. G. Yan, and P. T. Yu, Catalyst and Catalyst-Support Durability in *Handbook of Fuel Cells: Fundamentals Technology and Applications*, editors: W. Vielstich, H. Yokokawa, and H. A. Gasteiger, John Wiley & Sons (2009).
- K. Ota and Y. Koizumi, Platinum Dissolution Models and Voltage Cycling Effects: Platinum Dissolution in Polymer Electrolyte Fuel Cell (PEFC) and Low-temperature Fuel Cells in *Handbook of Fuel Cells: Fundamentals Technology and Applications*, editors: W. Vielstich, H. Yokokawa, and H. A. Gasteiger, John Wiley & Sons (2009).
- S. Mitsushima, Y. Koizumi, S. Uzuka, and K. I. Ota, *Electrochim. Acta*, **54**, 455 (2008).
- D. A. J. Rand and R. Woods, *J. Electroanal. Chem. Interfacial Electrochem.*, **35**, 209 (1972).
- K. Kinoshita, J. T. Lundquist, and P. Stonehart, *J. Electroanal. Chem. Interfacial Electrochem.*, **48**, 157 (1973).
- S. Mitsushima, S. Kawahara, K. I. Ota, and N. Kamiya, *J. Electrochem. Soc.*, **154**, B153 (2007).
- S. S. Kocha, Electrochemical Degradation: Electrocatalyst and Support Durability in *Polymer Electrolyte Fuel Cell Degradation*, editors: M. M. Mench, E. C. Kumbur, and T. N. Veziroglu, Academic Press (2012).
- W. Bi and T. F. Fuller, *J. Electrochem. Soc.*, **155**, B215 (2008).
- M. F. Mathias, R. Makharia, H. A. Gasteiger, J. J. Conley, T. J. Fuller, C. J. Gittleman, S. S. Kocha, D. P. Miller, C. K. Mittelsteadt, and T. Xie, *Electrochem. Soc. Interface*, **14**, 24 (2005).
- R. L. Borup, J. R. Davey, F. H. Garzon, D. L. Wood, and M. A. Inbody, *J. Power Sources*, **163**, 76 (2006).
- Z. Yang, S. Ball, D. Condit, and M. Gummalla, *J. Electrochem. Soc.*, **158**, B1439 (2011).
- R. K. Ahluwalia, S. Arisetty, J. K. Peng, R. Subbaraman, X. Wang, N. Kariuki, D. J. Myers, R. Mukundan, R. Borup, and O. Polevaya, *J. Electrochem. Soc.*, **161**, F291 (2014).
- M. Uchimura, S. Sugawara, Y. Suzuki, J. Zhang, and S. S. Kocha, *ECS Trans.*, **16**(2), 225 (2008).
- W. Bi, Q. Sun, Y. Deng, and T. F. Fuller, *Electrochim. Acta*, **54**, 1826 (2009).
- M. Matsumoto, T. Miyazaki, and H. Imai, *J. Phys. Chem. C*, **115**, 11163 (2011).
- M. Uchimura and S. S. Kocha, *ECS Trans.*, **11**(1), 1215 (2007).
- J. Zhang, B. A. Litterer, W. Gu, H. Liu, and H. A. Gasteiger, *J. Electrochem. Soc.*, **154**, B1006 (2007).
- W. Bi, G. E. Gray, and T. F. Fuller, *Electrochem. Solid-State Lett.*, **10**, B101 (2007).
- P. J. Ferreira and Y. Shao-Horn, *Electrochem. Solid-State Lett.*, **10**, B60 (2007).
- T. Takeshita, H. Murata, T. Hatanaka, and Y. Morimoto, *ECS Trans.*, **16**(2), 367 (2008).
- T. Nagai, H. Murata, and Y. Morimoto, *J. Electrochem. Soc.*, **161**, F789 (2014).
- R. M. Darling and J. P. Meyers, *J. Electrochem. Soc.*, **150**, A1523 (2003).
- R. M. Darling and J. P. Meyers, *J. Electrochem. Soc.*, **152**, A242 (2005).
- A. A. Franco and M. Tembely, *J. Electrochem. Soc.*, **154**, B712 (2007).
- A. A. Franco, P. Schott, C. Jallut, and B. Maschke, *J. Electrochem. Soc.*, **153**, A1053 (2006).
- W. Bi and T. F. Fuller, *J. Power Sources*, **178**, 188 (2008).
- E. F. Holby, W. C. Sheng, Y. Shao-Horn, and D. Morgan, *Energ. Environ. Sci.*, **2**, 865 (2009).
- R. K. Ahluwalia, S. Arisetty, X. Wang, X. Wang, R. Subbaraman, S. C. Ball, S. DeCrane, and D. J. Myers, *J. Electrochem. Soc.*, **160**, F447 (2013).
- E. F. Holby and D. Morgan, *J. Electrochem. Soc.*, **159**, B578 (2012).
- C. F. Wang, *Chem. Rev. (Washington, DC)*, **104**, 4727 (2004).
- L. Tang, B. Han, K. Persson, C. Friesen, T. He, K. Sieradzki, and G. Ceder, *J. Am. Chem. Soc.*, **132**, 596 (2010).
- M. C. Smith, J. A. Gilbert, J. R. Mawdsley, S. Seifert, and D. J. Myers, *J. Am. Chem. Soc.*, **130**, 8112 (2008).
- P. Bindra, S. J. Clouser, and E. Yeager, *J. Electrochem. Soc.*, **126**, 1631 (1979).
- W. Gu, D. R. Baker, Y. Liu, and H. A. Gasteiger, Chapter 43 in *Handbook of Fuel Cells – Fundamentals Technology and Applications*, Vol. 6 Advances in Electrocatalysis, Materials, Diagnostics and Durability, editors: H. A. Gasteiger, W. Vielstich, and H. Yokokawa, p. 631, John Wiley & Sons (2009).
- D. J. Myers, X. Wang, N. Kariuki, T. Nowicki, S. DeCrane, R. Subbaraman, R. Ahluwalia, and S. Arisetty, Polymer Electrolyte Fuel Cell Lifetime Limitations: The Role of Electrocatalyst Degradation, *US DOE Hydrogen Program and Vehicle Technologies Program Annual Merit Review and Peer Evaluation Meeting (Washington D.C.)*, 2012.
- H. Ju, H. Meng, and C. Y. Wang, *Int. J. Heat Mass Transfer*, **48**, 1303 (2005).
- Y. Wang and C. Y. Wang, *J. Power Sources*, **147**, 148 (2005).
- A. Z. Weber, R. L. Borup, R. M. Darling, P. K. Das, T. J. Dursch, W. Gu, D. Harvey, A. Kusoglu, S. Litster, M. M. Mench, R. Mukundan, J. P. Owejan, J. G. Pharoah, M. Secanell, and I. V. Zenyuk, *J. Electrochem. Soc.*, **161**, F1254 (2014).
- H. A. Gasteiger, J. E. Panels, and S. G. Yan, *J. Power Sources*, **127**, 162 (2004).
- E. Billy, F. Maillard, A. Morin, L. Guetaz, F. Emieux, C. Thuriel, P. Doppelt, S. Donet, and S. Mailley, *J. Power Sources*, **195**, 2737 (2010).
- M. Cavarroc, A. Ennadjaoui, M. Mougnot, P. Brault, R. Escalier, Y. Tessier, J. Durand, S. Roualdès, T. Sauvage, and C. Coutanceau, *Electrochem. Commun.*, **11**, 859 (2009).
- A. Ohma, T. Mashio, K. Sato, H. Iden, Y. Ono, K. Sakai, K. Akizuki, S. Takaichi, and K. Shinohara, *Electrochim. Acta*, **56**, 10832 (2011).
- W. Yoon and A. Z. Weber, *J. Electrochem. Soc.*, **158**, B1007 (2011).
- T. A. Greszler, D. Caulk, and P. Sinha, *J. Electrochem. Soc.*, **159**, F831 (2012).
- S. Jomori, N. Nonoyama, and Y. Yoshida, *J. of Power Sources*, **215**, 18 (2012).
- J. P. Owejan, J. E. Owejan, and W. Gu, *J. Electrochem. Soc.*, **160**, F824 (2013).
- S. Arisetty, X. Wang, R. K. Ahluwalia, R. Mukundan, R. Borup, J. Davey, D. Langlois, F. Gambini, O. Polevaya, and S. Blanchet, *J. Electrochem. Soc.*, **159**, B455 (2012).